PNAS RESEARCH ARTICLE | GENETICS

Mechanisms of photoreceptor protection upon targeting the *Nrl–Nr2e3* pathway

Daniel P. Murphy[a], Alexander V. Kolesnikov[b], Cynthia L. Montana[a,c], Zaid M. Khaja[a,d], Yu Liu[a], Vladimir J. Kefalov[b,e], and Joseph C. Corbo[a,1]

Affiliations are included on p. 9.

Edited by Jeremy Nathans, Johns Hopkins University School of Medicine, Baltimore, MD; received January 7, 2025; accepted April 7, 2025

Acute knockout of the rod photoreceptor transcription factor *Nrl* delays retinal degeneration in multiple mouse models of blindness, but the downstream transcriptomic changes that mediate these therapeutic effects are unknown. Here, we show that acute *Nrl* knockout causes upregulation of a subset of cone genes in rods as well as downregulation of rod genes, including the rod-specific transcriptional repressor *Nr2e3*. We hypothesized that *Nr2e3* downregulation might mediate some of the therapeutic effects of *Nrl* knockout. Indeed, acute knockout of *Nr2e3* prevents photoreceptor degeneration and preserves visual function in mice with mutations in the catalytic subunit of the rod-specific phosphodiesterase (*Pde6b*$^{rd10/rd10}$). Upregulation of *Pde6c*, the cone-specific paralog of *Pde6b*, in *Nr2e3*-knockout rods is required to prevent degeneration in *Pde6b*$^{rd10/rd10}$ mice, suggesting that this therapeutic effect is mediated, at least in part, by a gene-replacement mechanism. In contrast, acute *Nr2e3* knockout fails to prevent degeneration caused by loss- or gain-of-function mutations in Rhodopsin (*Rho*$^{-/-}$ and *Rho*$^{P23H/P23H}$), whereas acute *Nrl* knockout delays degeneration in both models. Surprisingly, the therapeutic effect of acute *Nrl* knockout in *Pde6b*$^{rd10/rd10}$ mice does not depend on *Pde6c* upregulation. These results suggest that acute *Nrl* knockout may exert its therapeutic effects via a mechanism independent of *Nr2e3* downregulation, perhaps by downregulating other rod genes. We conclude that acute *NRL* knockout may be a promising gene-independent strategy for preventing photoreceptor degeneration in human patients.

retina | photoreceptor | retinitis pigmentosa | Nrl | Nr2e3

Significance

Acute knockout of the rod-photoreceptor-specific transcription factor *Nrl* delays degeneration in multiple mouse models of retinitis pigmentosa (RP), but the downstream therapeutic mechanisms are unknown. Here, we show that acute knockout of the *Nrl* -downstream transcription factor *Nr2e3* is neuroprotective in mice with mutations in *Pde6b* but ineffective in two mouse models with mutations in *Rhodopsin*. The therapeutic effect in *Pde6b* mutant mice depends on upregulation of *Pde6c*. Conversely, *Nrl* knockout is effective in all three models, and rescue in *Pde6b* mutant mice is independent of *Pde6c* upregulation. These findings underscore the broad therapeutic efficacy of acute *Nrl* knockout and suggest that the effects of acute *Nrl* knockout are both overlapping and independent of those caused by acute *Nr2e3* knockout.

Retinal degeneration is a major cause of blindness afflicting millions of people worldwide (1–4). Retinitis pigmentosa (RP) is the most common form of retinal degeneration and can be caused by mutations in nearly 70 genes (2, 3). In RP, mutations in rod-expressed genes cause rod dysfunction and death, which is subsequently followed by secondary cone loss. The death of cones, which mediate daytime vision, is particularly disabling for patients and represents the primary source of morbidity in RP (2, 3). Preventing secondary cone loss is therefore a key goal of therapy for this disease, but the genetic heterogeneity of RP poses a fundamental challenge for the development of broadly applicable treatments. Thus, there is a strong motivation to develop gene- and mutation-independent therapies that could be used to treat diverse genetic forms of RP (5, 6).

We previously hypothesized that converting adult rods into cones—via knockout of the rod photoreceptor determinant *Nrl*—would make the cells resistant to the effects of mutations in rod-specific genes, thereby preventing secondary cone loss (7). To test this idea, we engineered a conditional allele of *Nrl* to acutely inactivate the gene in adult rods (7). Acute *Nrl* knockout converted the rods into hybrid photoreceptors expressing both rod and cone genes, and this cellular transformation delayed rod death and preserved native cones in a mouse model of RP (*Rho*$^{-/-}$) (7). Subsequent work by other groups replicated our findings and extended them to additional mouse models of RP (*Pde6b*$^{rd10/rd10}$ and *RHO*^{P347S} transgenic mice) (8, 9). Together, these studies demonstrated the first therapeutic effects that have ever been achieved via direct cellular reprogramming in the mammalian central nervous system and suggested that acute *Nrl* knockout may represent a promising gene-agnostic therapy for RP patients. Despite these advances, the downstream transcriptomic changes that mediate the therapeutic effects of acute *Nrl* knockout remain unknown. Furthermore, recent studies have reported a therapeutic effect upon both germline and acute knockout of the *Nrl*-downstream transcription factor *Nr2e3* (10, 11). Yet, the mechanistic relationship, if any, between the effects of *Nrl* and *Nr2e3* knockout have not been examined. The goal of the present study is to investigate these questions.

Author contributions: D.P.M., A.V.K., C.L.M., V.J.K., and J.C.C. designed research; D.P.M., A.V.K., C.L.M., Z.M.K., and Y.L. performed research; D.P.M., A.V.K., Z.M.K., Y.L., V.J.K., and J.C.C. analyzed data; and D.P.M., A.V.K., V.J.K., and J.C.C. wrote the paper.

The authors declare no competing interest.

This article is a PNAS Direct Submission.

[1]To whom correspondence may be addressed. Email: jcorbo@wustl.edu.

This article contains supporting information online at https://www.pnas.org/lookup/suppl/doi:10.1073/pnas.2500446122/-/DCSupplemental.

Published May 21, 2025.

Results

Transcriptomic Effects of Acute *Nrl* and *Nr2e3* Knockout. *Nrl* acts as a molecular toggle switch during retinal development: If a photoreceptor precursor turns on *Nrl*, it differentiates as a rod, otherwise it differentiates as a cone (12, 13). In contrast, acute *Nrl* knockout transforms mature rods into cells with features intermediate between those of normal rods and cones ("cods") (7). We previously showed by in situ hybridization that acute *Nrl* knockout causes upregulation of selected cone genes in rods and downregulation of a subset of rod genes (7). To more comprehensively evaluate the transcriptomic changes induced by acute *Nrl* knockout, we reexamined previously unpublished microarray data obtained at the time of our original study. In that analysis, we crossed mice carrying a "floxed" allele of *Nrl* with a transgenic line carrying a tamoxifen-inducible Cre recombinase (CAG-Cre^{ERTM}). We injected both experimental ($Nrl^{flox/flox}$; CAG-Cre^{ERTM}) and control ($Nrl^{flox/+}$; CAG-Cre^{ERTM}) mice daily with 4-hydroxytamoxifen from postnatal day 42 (P42) to 44, to induce acute *Nrl* knockout, and then harvested retinas at P63 and profiled them by microarray analysis in two biological replicates (Fig. 1*A*). In contrast to germline *Nrl* knockout which induces changes in the expression of nearly 2,000 genes (14), acute *Nrl* knockout alters the expression of only 144 genes (Fig. 1*B*). Approximately 38% (32 out of 85) of upregulated genes are enriched in adult cones, while 71% (42 out of 59) of downregulated genes are rod-enriched and include genes encoding components of the rod phototransduction cascade (*Rho*, *Gnat1*, and *Gnb1*) as well as the transcriptional repressor, *Nr2e3* (Dataset S1). The ability of NRL to repress cone genes in rods depends, in part, on induction of *Nr2e3* expression (Fig. 1*C*) (15–17). Germline mutation of *Nr2e3* in mice causes upregulation of diverse cone genes in rods but only modest effects on rod gene expression (16–18). Thus, analysis of acute *Nr2e3* knockout might permit us to determine whether cone gene upregulation or rod gene downregulation mediates the therapeutic effects observed upon acute *Nrl* knockout.

To acutely knock out *Nr2e3* in adult rods, we engineered an adeno-associated virus (AAV) carrying a guide RNA (gRNA) against *Nr2e3* and a photoreceptor-specific fluorescent reporter to label infected cells (Fig. 1*D*). We quantified the efficacy of

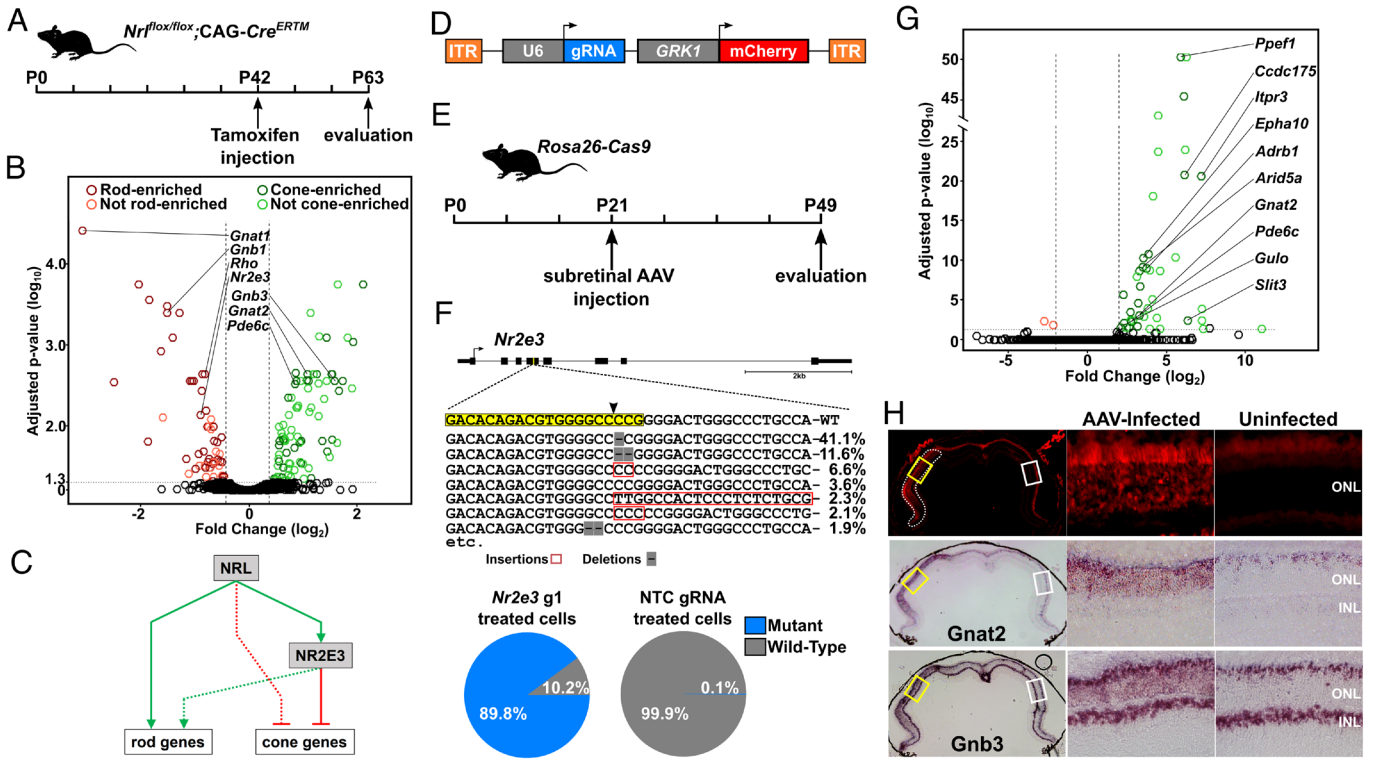

Fig. 1. Transcriptomic effects of acute *Nrl* and *Nr2e3* knockout. (*A*), Experimental timeline for expression profiling of acute *Nrl* knockout retinas by microarray. (*B*), Volcano plot showing gene expression changes in $Nrl^{flox/flox}$; CAG-Cre^{ERTM} retinas relative to controls ($Nrl^{flox/+}$; CAG-Cre^{ERTM}). Mice were given daily intraperitoneal injections of 4-hydroxytamoxifen from postnatal day 42 (P42) to 44, to induce acute *Nrl* knockout, and then whole retinas were harvested for microarray analysis at P63. Fold change and adjusted p-values were generated with *Limma* (19) based on two biological replicates for each condition. Dark green and dark red data points indicate genes that were previously shown to be enriched in adult cone and rod photoreceptors, respectively (14). Selected rod- and cone-enriched genes are labeled. (*C*), Schematic depicting the transcriptional regulatory network downstream of NRL in rods. Solid and dotted lines denote major and minor regulatory relationships, respectively. Green and red lines indicate activation and repression, respectively. (*D*), AAV construct used for acute *Nr2e3* knockout. (*E*), Experimental timeline for evaluating the efficiency of acute *Nr2e3* knockout. (*F*), *Top*: Schematic of the *Nr2e3* locus with a magnified view of the sequence around the gRNA target site (highlighted in yellow). *Middle*: The seven most common mutations identified in DNA from photoreceptors transduced with an AAV expressing *Nr2e3* g1. The predicted cut site is indicated by a black arrowhead. *Bottom*: Pie charts showing the percentage of mutant (blue) and wild-type (WT) (gray) sequence reads from cells treated with *Nr2e3* g1 or an NTC gRNA at P21 and harvested four weeks later. (*G*), Volcano plot showing gene expression changes in *Nr2e3* g1-treated photoreceptors relative to NTC-treated cells. One-month-old *Rosa26*-Cas9 mice were injected with AAV, infected cells were isolated 6 mo postinjection by fluorescence-activated cell sorting (FACS), and bulk RNA-seq analysis was performed. Color coding of dysregulated genes is as in *B*. Selected cone-enriched genes are labeled. The following categories of transcript were omitted from the plot for clarity: Long noncoding RNAs, pseudogenes, and those genes for which no rod or cone gene expression data were available (n = 19; all dysregulated genes are listed in Dataset S2). (*H*), In situ hybridization reveals upregulation of cone markers in rods upon acute *Nr2e3* knockout. The *Left* column shows sections of a whole retina infected with an AAV carrying *Nr2e3* g1 at one month of age and harvested 8 wks later. The area of AAV infection (indicated by mCherry expression) is highlighted with a white dotted line. Weak red autofluorescence is present throughout the outer segment layer, even in uninfected areas. Yellow and white boxes correspond to AAV-infected (*Middle* column) and uninfected regions (*Right* column), respectively. In situ hybridization shows expression of cone markers *Gnat2* and *Gnb3* throughout full thickness of the ONL, indicative of expression in rods. *Gnb3* is also expressed in bipolar cells in the INL. *Gnb3* is clearly upregulated in infected cells, although RNA-seq profiling (shown in *G*) failed to detect a statistically significant change in its expression. ONL, Outer nuclear layer; INL, Inner nuclear layer.

Nr2e3 knockout by injecting this virus into the subretinal space of P21 *Rosa26-Cas9* mice that express Cas9 in all cells and then used fluorescence-activated cell sorting (FACS) to isolate infected photoreceptors four weeks after injection (Fig. 1*E*). We performed PCR across the gRNA-targeted region using genomic DNA extracted from the sorted cells and found that 89.8% of all *Nr2e3* alleles contained a mutation (Fig. 1*F* and *SI Appendix*, Table S1). Next, we repeated this experiment, but this time we harvested retinas at six months post-injection and performed bulk RNA-seq analysis on the FACS-purified cells and compared their transcriptome to that of cells infected with a virus expressing a nontargeting control (NTC) gRNA. We found that only 66 genes changed expression by ≥2-fold (Fig. 1*G* and Dataset S2). Consistent with NR2E3's role as a transcriptional repressor (15–17), nearly all dysregulated genes were upregulated, and about one-third of these upregulated genes were cone-enriched (Fig. 1*G*). In situ hybridization for two cone-enriched genes (*Gnat2* and *Gnb3*) confirmed upregulation specifically in AAV-infected cells (Fig. 1*H*). In contrast, germline *Nr2e3* knockout alters the expression of 141 genes in mouse retina by ≥2-fold (Dataset S3) (18). Thus, both acute *Nrl* and *Nr2e3* knockouts have milder effects on gene expression than the corresponding germline knockouts.

Acute *Nr2e3* Knockout Prevents Degeneration in *Pde6b*$^{rd10/rd10}$ Mice. Next, we tested whether acute *Nr2e3* knockout could prevent photoreceptor degeneration in *Pde6b*$^{rd10/rd10}$ mice, a model of RP (20). *Pde6b* is a rod-specific gene which encodes part of the catalytic subunit of phosphodiesterase, an essential component of the rod phototransduction cascade (21). Mutations in *PDE6B* cause RP in humans (22), and *Pde6b*$^{rd10/rd10}$ mice display an early, rapid phase of rod loss starting around P15, followed by secondary cone death (Fig. 2*A*) (21, 23). By P60 essentially all rods are gone, and cone death is advancing (21). We previously showed that a germline mutation in *Nr2e3* (*rd7*) prevents photoreceptor degeneration in *Pde6b*$^{rd10/rd10}$ mice (10). Furthermore, another study suggested that acute *Nr2e3* knockout may be neuroprotective in this model as well as in FVB/N mice which are homozygous for the *rd1* allele of *Pde6b* (11). To more comprehensively evaluate the therapeutic effect of acute *Nr2e3* knockout, we injected *Rosa26-Cas9; Pde6b*$^{rd10/rd10}$ mice at P7 with an AAV carrying a gRNA targeting *Nr2e3* (g1) or an NTC gRNA and then harvested retinas for histologic evaluation at P60 (Fig. 2*A*). Retinas infected with the *Nr2e3* g1 virus showed excellent preservation of photoreceptors in the outer nuclear layer (ONL), including cones (Fig. 2*B* and *SI Appendix*, Fig. S1). In contrast, the ONL of NTC-infected retinas had degenerated to a single layer of cells lacking cone opsin immunoreactivity. To evaluate the durability of this therapeutic effect, we injected *Rosa26-Cas9; Pde6b*$^{rd10/rd10}$ mice at P15 with *Nr2e3* g1 virus or an NTC-control and quantified photoreceptors at P60 and P180. We observed persistent preservation of photoreceptors at P180 (*SI Appendix*, Fig. S2 *A–C*). Sequence analysis of *Nr2e3* g1-infected wild-type (WT) rods demonstrated mutations at a predicted off-target site deep within an intron of *Vps13b* (*SI Appendix*, Fig. S3*A*). To rule out the possibility that the therapeutic effect of *Nr2e3* g1 was mediated by off-target mutations, we repeated the experiment using a second *Nr2e3* gRNA (g2) with a distinct spectrum of predicted off-target sites (Fig. 3*B*). *Nr2e3* g2 showed therapeutic efficacy comparable to that of *Nr2e3* g1, indicating that the therapeutic effects are attributable to *Nr2e3* knockout (Fig. 2*B*). Finally, we performed the experiment using a gRNA against *Nrl* (g1) which showed highly efficient knockout (*SI Appendix*, Fig. S3*C*) and therapeutic efficacy comparable to that of the two *Nr2e3* gRNAs (Fig. 2*C*).

To determine whether acute *Nr2e3* knockout preserves photoreceptor function in *Pde6b*$^{rd10/rd10}$ mice, we performed in vivo electroretinography (ERG) recordings. We examined the function of rods and M-cones by determining the b-wave ERG response under scotopic and photopic conditions, respectively (Fig. 2*D*). To allow comparison with the morphological results, we performed the ERG recordings on 60-d-old *Rosa26*-Cas9; *Pde6b*$^{rd10/rd10}$ mice that had been injected with *Nr2e3* g1 at P7. Consistent with the observed morphological protection, animals with retinas infected with the *Nr2e3* g1 virus showed significantly larger ERG responses compared to their NTC-infected counterparts under both scotopic and photopic conditions (Fig. 2*D*). The extent of ERG rescue varied from eye to eye (*SI Appendix*, Fig. S2), which we attribute to variability in the extent of retinal surface area infected. Most retinas analyzed had ~25 to 30% of the retinal surface infected and the corresponding eyes showed moderate ERG rescue. In contrast, one eye with a particularly well-infected retina (i.e., with >90% of its surface area expressing mCherry) showed exceptional preservation of ERG responses (*SI Appendix*, Fig. S2 *D–F*, green trace). Taken together, these findings indicate that acute *Nr2e3* knockout preserves rod and cone photoreceptor function in *Pde6b*$^{rd10/rd10}$ mice.

To further quantify rescue of visual function, we evaluated treated mice using the Morris water maze, a test of vision-guided spatial learning. In this assay, a mouse is placed in a circular tub filled with opaque, milky water and must swim to a submerged platform marked by a red ball to "escape" from the water. Over the course of multiple trials, mice with intact vision learn to swim more directly toward the ball, while blind mice fail to learn the task (Fig. 2*E*). We evaluated three cohorts of 2-mo-old *Rosa26-Cas9; Pde6b*$^{rd10/rd10}$ mice which had been injected at P7 with an AAV either expressing the *Nr2e3* g1 gRNA or an NTC gRNA. We tested each mouse in two blocks per day for two consecutive days, each block consisting of two trails. In each trial, we measured swimming speed, total path length, and time required for the mouse to reach the hidden platform. A mixed-samples ANOVA revealed a significant difference between *Nr2e3* knockout mice and controls for both path length and time ($P = 5.0 \times 10^{-4}$ and $P = 1.0 \times 10^{-3}$, respectively; Fig. 2*E*), but no difference in swimming speed ($P = 0.5$). As expected, pairwise post hoc comparisons showed no difference between acute *Nr2e3* knockout and control mice for any measurement in the initial block of trials (i.e., before the mice learned the task). In contrast, in trial blocks 2 to 4, mice injected with *Nr2e3* g1 virus escaped over a shorter path and in less time than controls (Fig. 2*E*). Additionally, the *Nr2e3* knockout animals showed evidence of vision-based learning, as demonstrated by a shortening of both path length and escape time between blocks 1 and 4 ($P = 1.3 \times 10^{-4}$ and $P = 6.2 \times 10^{-5}$, respectively). Control mice showed no learning across trials. These results demonstrate that acute *Nr2e3* knockout preserves vision-guided behavior in *Pde6b*$^{rd10/rd10}$ mice.

Acute Knockout of *Nrl* but not *Nr2e3*, Delays Degeneration in *Rho* Mutants. We next evaluated the therapeutic efficacy of acute *Nr2e3* knockout in mice with loss- and gain-of-function mutations in Rhodopsin (*Rho*$^{-/-}$ and *Rho*$^{P23H/P23H}$, respectively) (24, 25). Rhodopsin conjugated to 11-*cis* retinal constitutes visual pigment, the light-sensing molecule of rods. Loss-of-function mutations in human *RHO* cause autosomal recessive RP, and the gain-of-function P23H mutation is the most common cause of autosomal dominant RP in human patients (26). *Rho*$^{-/-}$ mice show loss of rods starting around P30, followed by secondary cone death (Fig. 3*A*) (24, 27). By P90, almost all rods are gone, and cone dysfunction is advanced (27). We injected *H11*-Cas9*; Rho*$^{-/-}$ mice

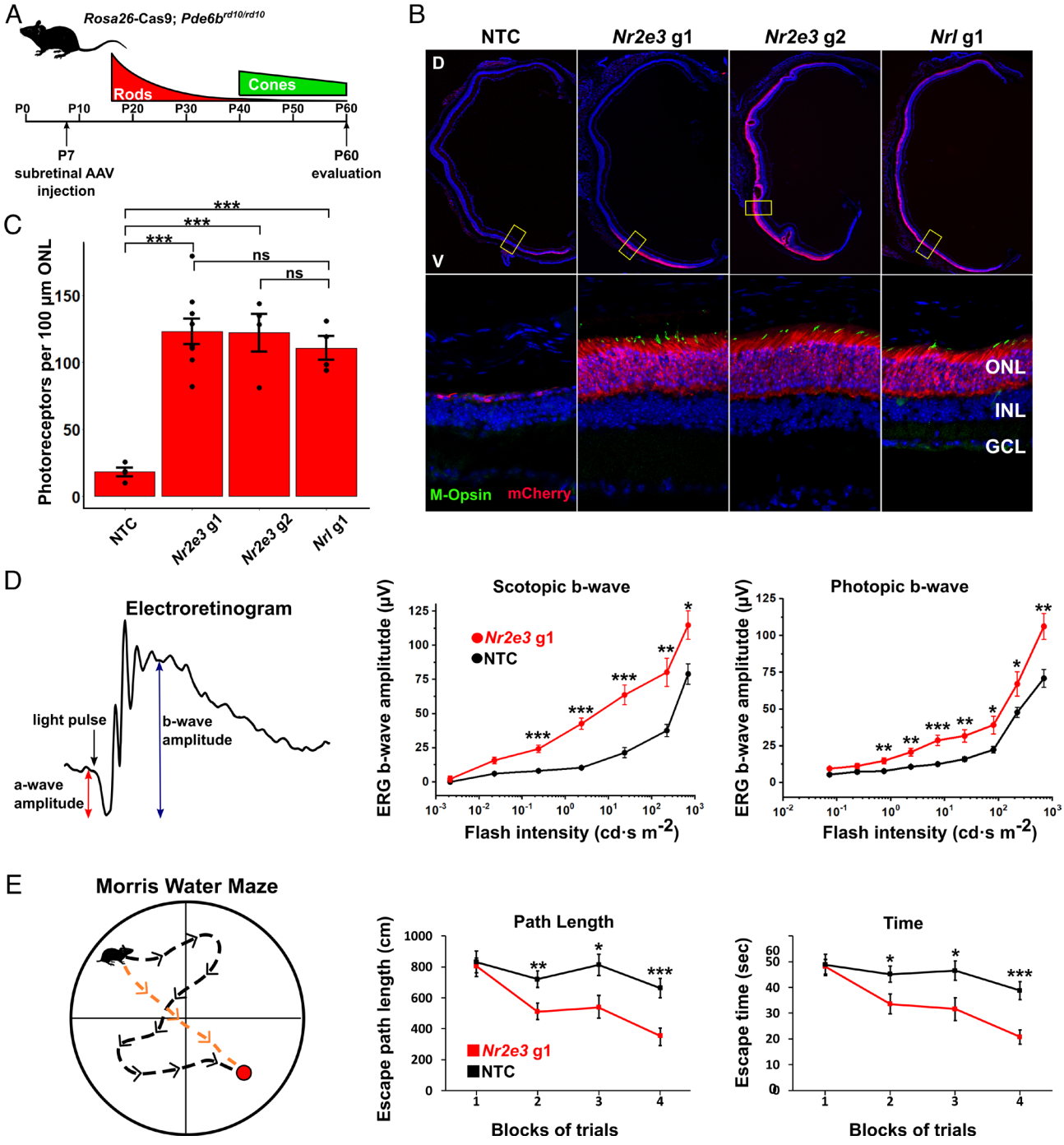

Fig. 2. Acute *Nr2e3* knockout prevents photoreceptor degeneration and preserves visual function in *Pde6b*$^{rd10/rd10}$ mice. (*A*), Experimental timeline for evaluating therapeutic efficacy of acute knockout in *Pde6b*$^{rd10/rd10}$ mice. The genotype of the injected mice and the temporal progression of rod and cone degeneration are shown. (*B*), Evaluation of histologic rescue upon acute *Nr2e3* or *Nrl* knockout. Whole-retina cross-sections (*Top* row) or close-ups (*Bottom* row; corresponding to the yellow box in *Top* row) show AAV-infected areas (indicated by mCherry expression) in retinas harvested at P60 from *Rosa26*-Cas9; *Pde6b*$^{rd10/rd10}$ mice injected at P7 with AAVs expressing the indicated gRNA. Immunohistochemistry for M-opsin is in green. D, dorsal; V, ventral; GCL, ganglion cell layer. (*C*), Quantification of results in *B*. Data are represented as mean ± SEM; individual values are shown as dots. Conditions were compared using an independent samples *t* test. (*D*), Evaluation of electrophysiologic rescue upon acute *Nr2e3* knockout. Example ERG trace is shown on the *Left*. Scotopic (*Middle* panel) and photopic (*Right* panel) b-wave measurements were obtained from in vivo ERGs performed at P60 on *Rosa26*-Cas9; *Pde6b*$^{rd10/rd10}$ mice injected with AAV expressing either *Nr2e3* g1 or an NTC gRNA at P7. Each flash intensity was compared using an independent samples *t* test. Data are presented as mean ± SEM (n = 9 for *Nr2e3* g1 and n = 10 for NTC gRNA). (*E*), Evaluation of vision-guided spatial learning after acute *Nr2e3* knockout. Experimental setup of the Morris water maze assay (*Left*). The total path length (*Middle* panel) and amount of time (*Right* panel) required to find the hidden platform decrease over successive trials in 2-mo-old *Rosa26*-Cas9; *Pde6b*$^{rd10/rd10}$ mice injected at P7 with AAV expressing *Nr2e3* g1 but not in those injected with AAV expressing an NTC gRNA. Successive trials were performed over the course of two days. Statistical significance was determined using a mixed samples ANOVA, n = 14 for *Nr2e3* g1 and n = 16 for NTC gRNA. For all statistical tests: **P* < 0.05, ***P* < 0.01, ****P* < 0.001.

at P21 with an AAV carrying a gRNA targeting *Nr2e3* or an NTC gRNA and then harvested retinas for histologic evaluation at P90. We used *H11*-Cas9 mice to express Cas9 because *Rho* and *Rosa26* are both located on mouse chromosome 6 and can therefore not be combined in the same animal. We found that acute knockout of *Nr2e3* failed to prevent retinal degeneration in *Rho*$^{-/-}$ mice (Fig. 3 *B* and *C*). In contrast, mice injected with a gRNA against *Nrl* showed substantial rescue of photoreceptors (Fig. 3 *B* and

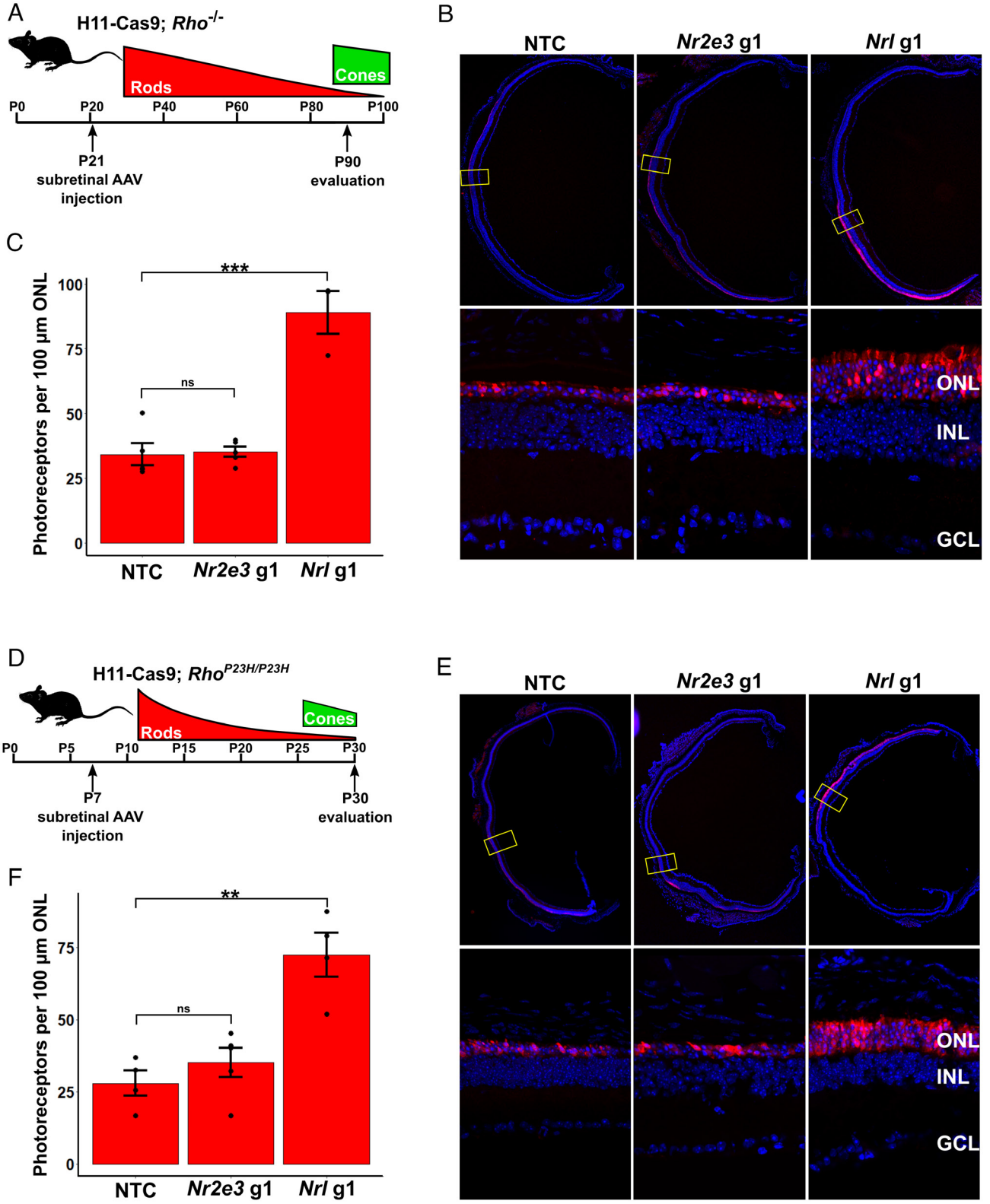

Fig. 3. Acute *Nrl* knockout, but not acute *Nr2e3* knockout, delays photoreceptor degeneration in *Rho* mutant mice. (*A*), Experimental timeline for evaluating therapeutic efficacy of acute knockout in $Rho^{-/-}$ mice. (*B*), Evaluation of histologic rescue upon acute *Nr2e3* or *Nrl* knockout. Whole-retina cross-sections (*Top* row) or close-ups (*Bottom* row; corresponding to the yellow box in *Top* row) show AAV-infected areas (indicated by mCherry expression) in retinas harvested at P90 from H11-Cas9; $Rho^{-/-}$ mice injected at P21 with AAVs expressing the indicated gRNA. (*C*), Quantification of results in *B*. Data are represented as mean ± SEM; individual values are shown as dots. Conditions were compared using an independent samples *t* test. (*D*), Experimental timeline for evaluating therapeutic efficacy of acute knockout in H11-Cas9;$Rho^{P23H/P23H}$ mice. (*E*), Evaluation of histologic rescue upon acute *Nr2e3* or *Nrl* knockout. Whole-retina cross-sections (*Top* row) or close-ups (*Bottom* row; corresponding to the yellow box in *Top* row) show AAV-infected areas (indicated by mCherry expression) in retinas harvested at P30 from H11-Cas9; $Rho^{P23H/P23H}$ mice injected at P7 with AAVs expressing the indicated gRNA. (*F*), Quantification of results in *E*. Data are represented as mean ± SEM; individual values are shown as dots. Conditions were compared using an independent samples *t* test. *$P < 0.05$, **$P < 0.01$, ***$P < 0.001$.

C), as previously reported (8). Next, we evaluated therapeutic efficacy in *Rho*$^{P23H/P23H}$ mice which experience rapid degeneration of rods starting shortly after P10; by P30, nearly all rods are gone and cone loss is progressing (Fig. 3*D*) (28). We injected P7 *H11-Cas9; Rho*$^{P23H/P23H}$ mice with an AAV carrying a gRNA targeting *Nr2e3*, *Nrl*, or an NTC gRNA and then harvested retinas for histologic evaluation at P30. Again, we found that acute knockout of *Nr2e3* failed to prevent photoreceptor degeneration while acute *Nrl* knockout afforded substantial neuroprotection (Fig. 3 *E* and *F*). Taken together, our findings indicate that acute *Nrl* knockout delays retinal degeneration in three mechanistically distinct RP models (*Pde6b*$^{rd10/rd10}$, *Rho*$^{-/-}$, and *Rho*$^{P23H/P23H}$), while acute *Nr2e3* knockout is protective in only one of them (*Pde6b*$^{rd10/rd10}$).

***Pde6c* Upregulation Mediates the Therapeutic Effect of *Nr2e3* Knockout.** Next, we sought to determine the mechanistic basis for the selectivity of *Nr2e3*-knockout-mediated rescue in *Pde6b*$^{rd10/rd10}$ mice. We hypothesized that one or more of the 63 genes upregulated upon acute *Nr2e3* knockout (Fig. 1*G*) might mediate the therapeutic effect. One promising candidate is *Pde6c*, which encodes the catalytic subunit of the cone-specific phosphodiesterase. Prior studies showed that ectopic expression of *Pde6c* in rods rescues degeneration in *Pde6b* mutant mice (29, 30). To determine whether increased levels of *Pde6c* transcripts correlate with increased protein expression after acute *Nr2e3* knockout, we used antibody staining to evaluate PDE6C levels in *Rosa26-Cas9* mice injected with *Nr2e3* gRNA g1 or an NTC gRNA. Consistent with our hypothesis (Fig. 4*A*), we found that acute *Nr2e3* knockout results in widespread upregulation of PDE6C in rod outer segments (Fig. 4*B*). If upregulation of *Pde6c* is required for the therapeutic effect of acute *Nr2e3* knockout, deletion of *Pde6c* should abrogate this effect. To test this idea, we generated mice with mutations in both *Pde6b* and *Pde6c* (*Rosa26-Cas9*; *Pde6b*$^{rd10/rd10}$; *Pde6c*$^{cpfl1/cpfl1}$), injected them at P7 with *Nr2e3* gRNA g1 or an NTC gRNA, and evaluated cellular rescue at P42 (Fig. 4*C*). We found that mutation of *Pde6c* largely abrogates the therapeutic effect of acute *Nr2e3* knockout, but some residual histologic rescue persists (Fig. 4*D*, orange bars in *E*). To determine the proportion of cellular rescue which is dependent on *Pde6c* upregulation, we repeated the experiment in mice with intact *Pde6c* (Fig. 4*D*, red bars in *E*). We found that approximately 83% of the cellular rescue is dependent on *Pde6c* upregulation, and the remainder is *Pde6c*-independent (Fig. 4*E* and *Materials and Methods*). Acute *Nrl* knockout causes downregulation of *Nr2e3* and corresponding upregulation of *Pde6c* (Fig. 1*B*), suggesting that it may mediate rescue in the *Pde6b*$^{rd10/rd10}$ model by a similar mechanism. To test this hypothesis, we repeated the experiment, this time with *Nrl* g1. Surprisingly, *Pde6c* deficiency did not diminish the therapeutic effect of acute *Nrl* knockout (Fig. 4 *D* and *E*). Taken together, these results indicate that in the *Pde6b*$^{rd10/rd10}$ degeneration model, the therapeutic effect of acute *Nr2e3* knockout is mediated by a combination of *Pde6c*-dependent and *Pde6c*-independent mechanisms, whereas the therapeutic effect of acute *Nrl* knockout is independent of *Pde6c* upregulation.

Discussion

Targeting the *Nrl–Nr2e3* pathway—either by germline or acute knockout—delays photoreceptor degeneration in multiple mouse models of RP (Fig. 4*F*) (7–9, 11). Here, we confirm that acute *Nrl* knockout is neuroprotective in three models (*Rho*$^{-/-}$, *Rho*$^{P23H/P23H}$, and *Pde6b*$^{rd10/rd10}$), while acute *Nr2e3* knockout prevents retinal degeneration in only one (*Pde6b*$^{rd10/rd10}$) (Fig. 4*F*). The therapeutic effect in *Pde6b*$^{rd10/rd10}$ mice is largely mediated by upregulation of *Pde6c* in rods, suggesting a "gene replacement" mechanism. We previously reported that germline *Nr2e3* knockout is neuroprotective in three models of photoreceptor degeneration (light damage, *Rho*$^{-/-}$, and *Pde6b*$^{rd10/rd10}$) (10). Thus, rescue of degeneration in *Pde6b*$^{rd10/rd10}$ is the only therapeutic effect shared by all three knockouts (i.e., acute *Nrl*, acute *Nr2e3*, and germline *Nr2e3*) (Fig. 4*F*). A comparison of transcriptomic changes in these three knockouts reveals only four upregulated genes in common (*Ccdc175*, *Clca1*, *Gnat2*, and *Pde6c*) (*SI Appendix*, Fig. S4), raising the possibility that *Pde6c* upregulation might represent a shared therapeutic mechanism in *Pde6b*$^{rd10/rd10}$ mice. Surprisingly, rescue by acute *Nrl* knockout was independent of *Pde6c* upregulation. This result and the broader therapeutic efficacy of acute *Nrl* knockout compared to acute *Nr2e3* knockout implies the existence of alternative therapeutic mechanisms downstream of acute *Nrl* knockout. It remains to be determined whether the therapeutic efficacy in *Rho* mutants (and potentially other models) is attributable to upregulation of additional cone genes in rods or downregulation of rod genes, but a recent study points to the latter (31) (see below). In either case, the present results define a testable list of alternate candidate effector genes and reconfirm the broad therapeutic efficacy of acute *Nrl* knockout.

A prior study reported morphologic and electroretinographic rescue of *Pde6b*$^{rd10/rd10}$ and FVB/N mice (which are homozygous for the *rd1* allele of *Pde6b*) via acute *Nr2e3* knockout (11). Our study expands upon these findings in four ways: We evaluate the therapeutic efficacy of acute *Nr2e3* knockout in two additional models, *Rho*$^{-/-}$ and *Rho*$^{P23H/P23H}$; we include results of a Morris water maze assay for rescue in *Pde6b*$^{rd10/rd10}$; we demonstrate the dependence of the rescue in *Pde6b*$^{rd10/rd10}$ on upregulation of *Pde6c*; and we present RNA-seq analysis of the gene expression changes that occur downstream of acute *Nr2e3* knockout. While our findings suggest that the therapeutic efficacy of acute *Nr2e3* knockout may be restricted to a single mouse mutant, *NR2E3* mutations in human appear to have more widespread effects on rod gene expression than in mouse (32). Thus, acute *NR2E3* knockout in human rods may have broader therapeutic potential.

A recent study showed that photoregulin3—a small molecule that putatively acts as a modulator of NR2E3—causes selective downregulation of rod genes and delays photoreceptor loss in *Rho*$^{P23H/P23H}$ mice (31). The downregulation of rod genes after photoregulin3 treatment contrasts with the almost exclusive upregulation of cone genes we observed upon acute *Nr2e3* knockout. The reason for this discrepancy remains unclear. Nonetheless, downregulation of a similar set of rod genes (e.g., *Rho*, *Gnat1*, *Pde6g*, etc.) after photoregulin3 treatment and acute *Nrl* knockout suggests that rod gene downregulation may be responsible for the delay in photoreceptor degeneration observed in *Rho*$^{P23H/P23H}$ mice after both treatments.

Another recent study suggested that overexpression of *Nr2e3* in mouse rods slows disease progression in multiple RP models, including *Rho*$^{-/-}$, *Rho*$^{P23H/+}$, and *Pde6b*$^{rd1/rd1}$ (33). We find these results to be unconvincing as the histologic images (their Fig. 4*A*) show no appreciable difference in ONL thickness between treated mice and controls, despite the authors' claims to the contrary (their Fig. 4*C*). More systematic analysis of the therapeutic efficacy of *Nr2e3* overexpression is warranted since clinical trials are currently underway in patients with RP and Leber congenital amaurosis (34).

Taken together, these findings suggest that targeting the *NRL–NR2E3* pathway may be a viable approach to treating multiple genetically and mechanistically distinct forms of RP in human patients. We find that multiple downstream therapeutic effectors

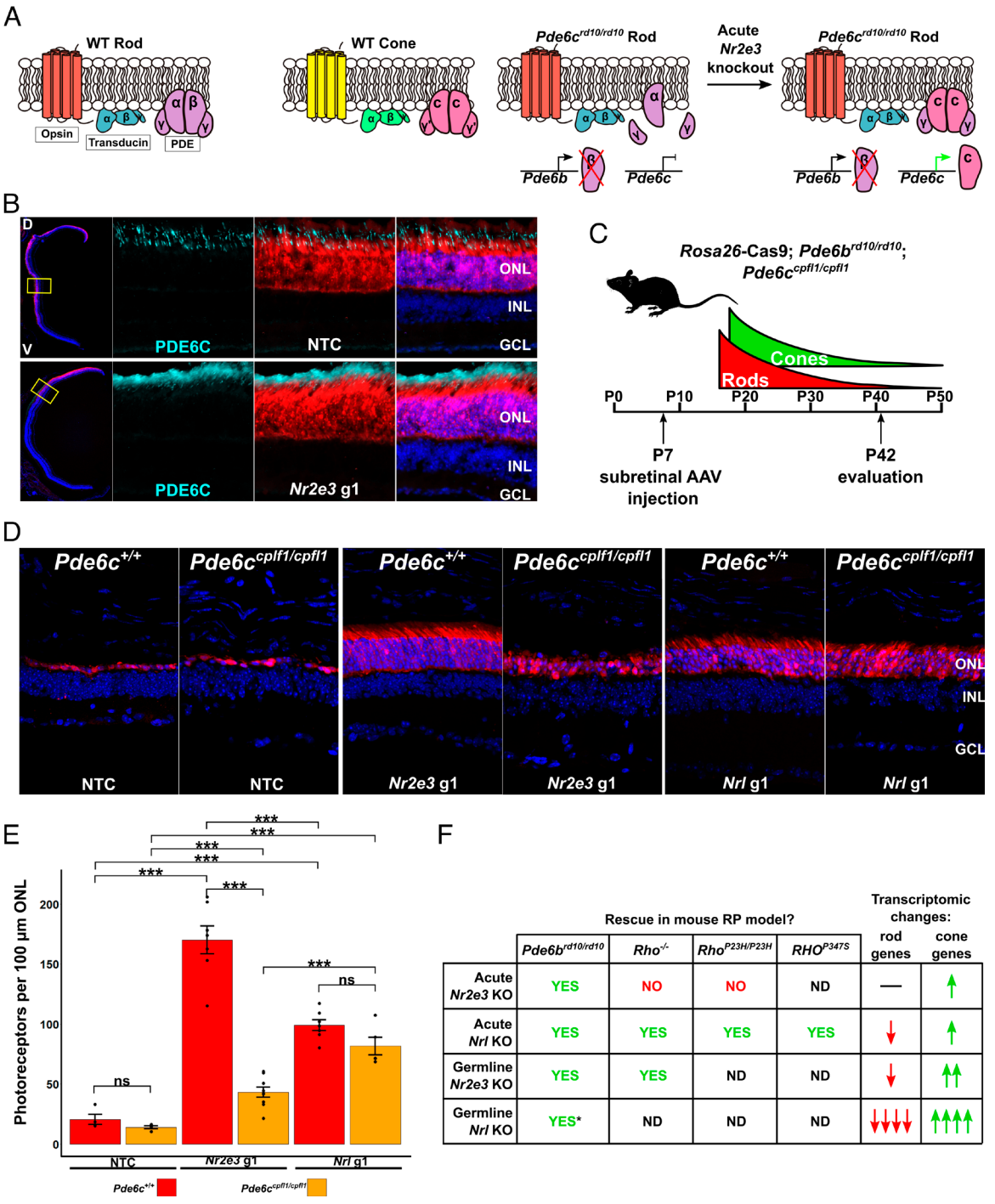

	Rescue in mouse RP model?				Transcriptomic changes:	
	Pde6b$^{rd10/rd10}$	*Rho*$^{-/-}$	*Rho*$^{P23H/P23H}$	*RHO*^{P347S}	rod genes	cone genes
Acute *Nr2e3* KO	YES	NO	NO	ND	—	↑
Acute *Nrl* KO	YES	YES	YES	YES	↓	↑
Germline *Nr2e3* KO	YES	YES	ND	ND	↓	↑↑
Germline *Nrl* KO	YES*	ND	ND	ND	↓↓↓↓	↑↑↑↑

Fig. 4. Upregulation of *Pde6c* after acute *Nr2e3* knockout prevents photoreceptor degeneration in *Pde6b*$^{rd10/rd10}$ mice. (*A*), Hypothesized mechanism of rescue by acute *Nr2e3* knockout. WT rods and cones express distinct opsin, transducin, and phosphodiesterase (PDE) components (*Top* row). *Pde6b*$^{rd10/rd10}$ mice express an unstable form of the β-subunit of rod phosphodiesterase (*Bottom* row). Upon acute *Nr2e3* knockout, *Pde6c* expression is upregulated in rods, thereby reconstituting a fully functional hybrid phosphodiesterase (*Bottom* row). (*B*), Antibody staining demonstrates PDE6C expression in *Nr2e3*-knockout rods. *Rosa26*-Cas9 mice were injected with either *Nr2e3* g1 or an NTC gRNA at P7, and retinas were harvested, sectioned, and stained at ~8 mo postinjection. Acute *Nr2e3* knockout (*Bottom* row) results in a continuous band of PDE6C staining in the outer segment layer consistent with its expression in rods, whereas retinas infected with an AAV expressing an NTC gRNA show staining restricted to cone outer segments (*Top* row). (*C*), Experimental timeline for evaluating therapeutic efficacy of acute knockout in *Pde6b*$^{rd10/rd10}$; *Pde6c*$^{cpfl1/cpfl1}$ mice. (*D*), The full therapeutic effect of acute *Nr2e3* knockout in *Pde6b*$^{rd10/rd10}$ mice depends on *Pde6c*. *Rosa26*-Cas9; *Pde6b*$^{rd10/rd10}$; *Pde6c*$^{cpfl1/cpfl1}$ mice were injected with AAV expressing either *Nr2e3* g1, *Nrl* g1, or an NTC gRNA at P7, and retinas were harvested for histologic evaluation at P42. Only the *Pde6c* genotype is indicated at the *Top*. (*E*), Quantification of results in *D*. *Pde6c* deficiency greatly diminishes the therapeutic effect of acute *Nr2e3* knockout, but some residual rescue remains. Conversely, the therapeutic effect of acute *Nrl* knockout is independent of *Pde6c*. The therapeutic effect of acute *Nr2e3* knockout is greater than that of acute *Nrl* knockout at this time point. Data are represented as mean ± SEM; individual values are shown as dots. Conditions were compared using an independent samples *t* test. (*F*), Summary of transcriptomic changes and therapeutic effects of germline or acute knockout of *Nr2e3* or *Nrl* in four different mouse models of RP with mutations in phototransduction components. The asterisk indicates that rescue was shown in *Pde6b*$^{rd1/rd1}$ mice, which display a more rapid degeneration than *Pde6b*$^{rd10/rd10}$ mice. ND, not done. *$P < 0.05$, **$P < 0.01$, ***$P < 0.001$.

are operative in distinct mouse models, and the same may prove true in humans. In *Pde6b*$^{rd10/rd10}$ mice, the most potent therapeutic effect depends, at least in part, on upregulation of *Pde6c*, which encodes the cone-specific paralog of *Pde6b*. This mechanism—induced upregulation of the "cone equivalent" of a rod-specific gene—is analogous to a recently reported treatment strategy in which the authors used CRISPR-mediated gene activation to upregulate the cone-specific M-opsin gene (*Opn1mw*) in the rods of *Rho*$^{-/-}$ mice (35). The latter strategy requires delivery of a catalytically "dead" Cas9 fused to a transcriptional activation domain via a "split" dual AAV system. The general applicability of this "gain-of-function" approach could be limited by the efficiency of dual AAV delivery and the extent of target gene upregulation achievable by CRISPR activation. In contrast, the *Nrl*–*Nr2e3* pathway can be targeted using small molecules—as shown with photoregulin3—or potentially via intraocular delivery of antisense oligonucleotides against *Nrl* or *Nr2e3*. Antisense oligonucleotides have shown considerable promise in the treatment of neurological diseases (36–38). Furthermore, this strategy has the added advantage over AAV-based therapies that treatment can be discontinued if adverse side effects occur.

Materials and Methods

Animals. Animals were fed with standard chow (LabDiet 5053; Purina Mills, Gray Summit, MO) and raised under a 12-h dark/light cycle. Experimental procedures were carried out in accordance with the NIH Guide for the Care and Use of Laboratory Animals and the ARVO Statement for the Use of Animals in Ophthalmic and Vision Research and were approved by the Institutional Animal Care and Use Committee of Washington University in St. Louis (protocol #22-0430). Additional details are provided in *SI Appendix, Materials and Methods*.

Genotyping. All mouse genotyping reactions were performed according to established protocols (20, 24, 25, 39, 40) except for *Pde6c*$^{cpfl1/cpfl1}$mice (41). In this case, DNA primers (listed in *SI Appendix*, Table S2) were used to amplify a 312 bp region encompassing a 1 bp deletion in exon 7 of *Pde6c*^{cpfl1} which generates a unique *Fok*1 site (GGATG). Additional details are provided in *SI Appendix, Materials and Methods*.

AAV Vectors. The vector for delivery of CRISPR gRNAs was modified from pAAV-U6-gRNA-CBh-mCherry (a gift from Jimok Kim; Addgene plasmid # 91947) (42). The NTC gRNA sequence (GCTTTCACGGAGGTTCGACG) was selected from the GeCKO v2 mouse library (43). The gRNA targeting *Nrl* (GTATGGTGTGGAGCCCAACG) is the same one used in a previous study (8). All oligonucleotides used for cloning guide RNAs are listed in *SI Appendix*, Table S2. Additional details are provided in *SI Appendix, Materials and Methods*.

AAV Vector Packaging. AAV genomes were packaged with a 7m8 coat (44) according to a standard procedure. Additional details are provided in *SI Appendix, Materials and Methods*.

Subretinal Injection of AAV. Subretinal AAV injections were performed either manually or with the aid of a stereotactic apparatus. Additional details are provided in *SI Appendix, Materials and Methods*.

ERG. Mice were dark-adapted overnight and anesthetized with an intraperitoneal injection of ketamine (100 mg/kg) and xylazine (4 mg/kg). Scotopic and photopic ERG responses were measured from both eyes. Further details are provided in *SI Appendix, Materials and Methods*.

Morris Water Maze Assay. The Morris water maze assay was performed as described previously (45) with some modifications as described in *SI Appendix, Materials and Methods*.

Retinal Dissociation and FACS. Retinas isolated from AAV-injected mice were dissociated using papain incubation followed by trituration with additional details provided in *SI Appendix, Materials and Methods*. The filtered cells were sorted using an Aria II FACS machine (BD Biosciences, Franklin Lakes, NY) with appropriate gating based on forward scatter, side scatter, and mCherry fluorescence.

Evaluation of gRNA Efficacy. To assess gRNA efficacy, genomic DNA was purified from FAC sorted cells using the Qiagen DNEasy Blood and tissue kit (Qiagen; Germantown, MD). Library preparation and sequencing are described in detail in *SI Appendix, Materials and Methods*. The paired-end reads, amplicon sequences, and original gRNA target sequences were used as input to *CRISPResso2* with default parameter settings (46). The results of *CRISPResso2* for each gRNA at each target site are summarized in *SI Appendix*, Table S1.

RNA Sequencing. AAV-infected photoreceptor cells were sorted by FACS and collected into TRIzol LS reagent (Thermo Fisher Scientific, Waltham, MA). Total RNA was then purified according to the manufacturer's instructions. Details on RNA quality control, library preparation, and sequencing are available in *SI Appendix, Materials and Methods*. Paired-end reads were aligned to the mouse genome (GRCm38/mm10) using *STAR* (v2.7.3a) (47). Read counts were calculated using *HTSeq* (0.12.4) (48). Differential gene expression was calculated using *DESeq2* (v1.42.0) (49), requiring a minimum $\log_2$ fold-change of 1 and an adjusted p-value of 0.05. Previously published RNA-seq data from *Nr2e3*$^{rd7/rd7}$ and WT retina (18) were reprocessed in parallel using identical methods. The results of these analyses are presented in Datasets S2 and S3. Sequence data for acute *Nr2e3* knockout have been deposited in the NCBI Gene Expression Omnibus (GEO) and are available under accession GSE256407.

Microarray Analysis. *Nrl*$^{flox/flox}$; CAG-*Cre*^{ERTM} and *Nrl*$^{flox/+}$; CAG-*Cre*^{ERTM} mice were injected intraperitoneally on a daily basis from P42 to P44 with 4-hydroxytamoxifen (dissolved in 15% ethanol/85% corn oil; Sigma Aldrich, St. Louis, MO) to induce recombination of the *Nrl*^{flox} alleles, and retinas were then harvested at P63 for microarray analysis. Total RNA was extracted from retinas using TRIzol LS reagent (Thermo Fisher Scientific; Waltham, MA) and purified using the RNeasy kit (Qiagen; Germantown, MD). Two biological replicates, each consisting of total RNA from four retinas (two animals), for each genotype were analyzed. Details on target preparation, hybridization, and differential expression analysis are provided in *SI Appendix, Materials and Methods*. The results of this analysis are presented in Dataset S1. Microarray data have been deposited in GEO and are available under accession GSE256408.

Histology. Eyes were fixed, embedded in Optimal Cutting Temperature compound (OCT; Sakura Finetek USA; Torrance, CA), sectioned, mounted, and imaged using either an Olympus BX51 compound microscope or a Zeiss 880 laser-scanning confocal microscope in the Washington University Center for Cellular Imaging (WUCCI) at Washington University in St. Louis. Further details are provided in *SI Appendix, Materials and Methods*.

Quantification of Photoreceptor Cells. Photoreceptor nuclei were quantified in AAV-infected (i.e., mCherry^{+}) regions of the central or mid-peripheral retinas of AAV-injected mice. Sections in which the ONL was severely detached from the retinal pigment epithelium were excluded from the analysis. Further details are provided in *SI Appendix, Materials and Methods*.

Immunohistochemistry. Immunohistochemistry against PDE6C was performed on retinal sections from *Rosa26*-Cas9 mice injected subretinally at three weeks of age with AAV expressing either *Nr2e3* g1 or a NTC gRNA and harvested eight months later. Immunohistochemistry against M-opsin and S-opsin was performed on sections from *Rosa26*-Cas9; *Pde6b*$^{rd10/rd10}$ mice injected subretinally at P7 with AAV expressing gRNA targeting *Nr2e3*, *Nrl*, or control, and harvested at P60. Further details are provided in *SI Appendix*, SI *Materials and Methods*.

In Situ Hybridization. In situ hybridizations were performed as previously described (50). The retinal frozen sections used for the procedure derive from *Rosa26*-Cas9 mice injected subretinally at P30 with AAV expressing either *Nr2e3* g1 or a NTC gRNA and harvested eight weeks later. Antisense RNA riboprobes for *Gnat2* and *Gnb3* were synthesized from templates generated by PCR using mouse retinal cDNA and primers listed in *SI Appendix*, Table S2.

Data, Materials, and Software Availability. Sequencing data and Microarray and RNA-seq data have been deposited in NCBI Gene Expression Omnibus under accession numbers GSE256407 (51) and GSE256408 (52). All study data are included in the article and/or supporting information.

ACKNOWLEDGMENTS. We thank Y. Ogawa for critical reading of the manuscript. The PDE6C antibody was a gift from Dr. Visvanathan Ramamurthy (West

Virginia University). For assistance with next-generation sequencing, we thank the Genome Technology Access Core in the Department of Genetics as well as the DNA Sequencing Innovation Lab in the Center for Genome Sciences & Systems Biology, both at Washington University in St. Louis. We also thank the Flow Cytometry Core in the Department of Pathology and Immunology at Washington University in St. Louis for assistance with FACS analysis. Finally, we thank Dr. David Wozniak and the Animal Behavior Core (ABC) at Washington University in St. Louis for assistance with the Morris water maze assays. The ABC is supported by funds provided by the McDonnell Center for Systems Neuroscience, McDonnell Center for Cellular and Molecular Neuroscience, and the Taylor Family Institute at Washington University in St. Louis. This work was supported by the NIH (EY030075 and EY033810) and Washington University's Hope Center for Neurological Disorders. We also acknowledge support to the Gavin Herbert Eye Institute at the University of California, Irvine from an unrestricted grant from Research to Prevent Blindness and from NIH core Grant P30 EY034070.

Author affiliations: [a]Department of Pathology and Immunology, Washington University School of Medicine, St. Louis, MO 63110; [b]Gavin Herbert Eye Institute, Department of Ophthalmology, University of California, Irvine, CA 92617; [c]Department of Ophthalmology, Washington University School of Medicine, St. Louis, MO 63110; [d]Saint Louis University School of Medicine, St. Louis, MO 63104; and [e]Department of Physiology and Biophysics, University of California, Irvine, CA 92617

1. A. Rattner, H. Sun, J. Nathans, Molecular genetics of human retinal disease. *Annu. Rev. Genet.* **33**, 89–131 (1999).
2. A. I. den Hollander, A. Black, J. Bennett, F. P. Cremers, Lighting a candle in the dark: Advances in genetics and gene therapy of recessive retinal dystrophies. *J. Clin. Invest.* **120**, 3042–3053 (2010).
3. S. K. Verbakel *et al.*, Non-syndromic retinitis pigmentosa. *Prog. Retin. Eye Res.* **66**, 157–186 (2018).
4. N. Schneider *et al.*, Inherited retinal diseases: Linking genes, disease-causing variants, and relevant therapeutic modalities. *Prog. Retin. Eye Res.* **89**, 101029 (2022).
5. M. Zuzic *et al.*, Gene-independent therapeutic interventions to maintain and restore light sensitivity in degenerating photoreceptors. *Prog. Retin. Eye Res.* **90**, 101065 (2022), 10.1016/j.preteyeres.2022.101065.
6. M. C. John, J. Quinn, M. L. Hu, J. Cehajic-Kapetanovic, K. Xue, Gene-agnostic therapeutic approaches for inherited retinal degenerations. *Front. Mol. Neurosci.* **15**, 1068185 (2023).
7. C. L. Montana *et al.*, Reprogramming of adult rod photoreceptors prevents retinal degeneration. *Proc. Natl. Acad. Sci. U.S.A.* **110**, 1732–1737 (2013).
8. W. Yu *et al.*, Nrl knockdown by AAV-delivered CRISPR/Cas9 prevents retinal degeneration in mice. *Nat. Commun.* **8**, 14716 (2017).
9. A. M. Moreno *et al.*, In situ gene therapy via AAV-CRISPR-Cas9 mediated targeted gene regulation. *Mol. Ther.* **26**, 1818–1827 (2018), 10.1016/j.ymthe.2018.04.017.
10. A. V. Kolesnikov, D. P. Murphy, J. C. Corbo, V. J. Kefalov, Germline knockout of Nr2e3 protects photoreceptors in three distinct mouse models of retinal degeneration. *Proc. Natl. Acad. Sci. U.S.A.* **121**, e2316118121 (2024).
11. J. Zhu *et al.*, Gene and mutation independent therapy via CRISPR-Cas9 mediated cellular reprogramming in rod photoreceptors. *Cell Res.* **27**, 830–833 (2017).
12. L. L. Daniele *et al.*, Cone-like morphological, molecular, and electrophysiological features of the photoreceptors of the *Nrl* knockout mouse. *Invest. Ophthalmol. Visual Sci.* **46**, 2156–2167 (2005).
13. A. J. Mears *et al.*, Nrl is required for rod photoreceptor development. *Nat. Genet.* **29**, 447–452 (2001).
14. A. E. Hughes, J. M. Enright, C. A. Myers, S. Q. Shen, J. C. Corbo, Cell type-specific epigenomic analysis reveals a uniquely closed chromatin architecture in mouse rod photoreceptors. *Sci. Rep.* **7**, 43184 (2017).
15. J. C. Corbo, C. L. Cepko, A hybrid photoreceptor expressing both rod and cone genes in a mouse model of enhanced S-cone syndrome. *PLoS Genet.* **1**, e11 (2005).
16. J. Chen, A. Rattner, J. Nathans, The rod photoreceptor-specific nuclear receptor Nr2e3 represses transcription of multiple cone-specific genes. *J. Neurosci.: Off. J. Soc. Neurosci.* **25**, 118–129 (2005).
17. G. H. Peng, O. Ahmad, F. Ahmad, J. Liu, S. Chen, The photoreceptor-specific nuclear receptor Nr2e3 interacts with Crx and exerts opposing effects on the transcription of rod versus cone genes. *Hum. Mol. Genet.* **14**, 747–764 (2005).
18. Y. Xue *et al.*, The role of retinol dehydrogenase 10 in the cone visual cycle. *Sci. Rep.* **7**, 2390 (2017).
19. M. E. Ritchie *et al.*, limma powers differential expression analyses for RNA-sequencing and microarray studies. *Nucleic Acids Res.* **43**, e47 (2015).
20. B. Chang *et al.*, Retinal degeneration mutants in the mouse. *Vision Res.* **42**, 517–525 (2002).
21. B. Chang *et al.*, Two mouse retinal degenerations caused by missense mutations in the β-subunit of rod cGMP phosphodiesterase gene. *Vision Res.* **47**, 624–633 (2007).
22. L. Kuehlewein *et al.*, Clinical phenotype of PDE6B-associated retinitis pigmentosa. *Int. J. Mol. Sci.* **22**, 2374 (2021).
23. M. Samardzija *et al.*, Activation of survival pathways in the degenerating retina of rd10 mice. *Exp. Eye Res.* **99**, 17–26 (2012).
24. J. Lem *et al.*, Morphological, physiological, and biochemical changes in rhodopsin knockout mice. *Proc. Natl. Acad. Sci. U.S.A.* **96**, 736–741 (1999).
25. S. Sakami *et al.*, Probing mechanisms of photoreceptor degeneration in a new mouse model of the common form of autosomal dominant retinitis pigmentosa due to P23H opsin mutations. *J. Biol. Chem.* **286**, 10551–10567 (2011).
26. D. Athanasiou *et al.*, The molecular and cellular basis of rhodopsin retinitis pigmentosa reveals potential strategies for therapy. *Prog. Retin. Eye Res.* **62**, 1–23 (2018).
27. C. Punzo, K. Kornacker, C. L. Cepko, Stimulation of the insulin/mTOR pathway delays cone death in a mouse model of retinitis pigmentosa. *Nat. Neurosci.* **12**, 44–52 (2009).
28. W. C. Chiang *et al.*, Robust endoplasmic reticulum-associated degradation of *Rhodopsin* precedes retinal degeneration. *Mol. Neurobiol.* **52**, 679–695 (2015).
29. W. T. Deng *et al.*, Cone phosphodiesterase-6α′ restores rod function and confers distinct physiological properties in the rod phosphodiesterase-6β-deficient rd10 mouse. *J. Neurosci.: Off. J. Soc. Neurosci.* **33**, 11745–11753 (2013).
30. A. Majumder *et al.*, Exchange of cone for rod phosphodiesterase 6 catalytic subunits in rod photoreceptors mimics in part features of light adaptation. *J. Neurosci.: Off. J. Soc. Neurosci.* **35**, 9225–9235 (2015).
31. P. A. Nakamura *et al.*, Small molecule Photoregulin3 prevents retinal degeneration in the *Rho*^{P23H} mouse model of retinitis pigmentosa. *eLife* **6**, e30577 (2017).
32. K. M. Nathaniel *et al.*, Loss of NR2E3 disrupts rod photoreceptor cell maturation causing a fate switch late in human retinal development. bioXriv [Preprint] (2023), 10.1101/2023.06.30.547279.
33. S. Li *et al.*, Nr2e3 is a genetic modifier that rescues retinal degeneration and promotes homeostasis in multiple models of retinitis pigmentosa. *Gene Ther.* **28**, 223–241 (2021).
34. Anonymous, "NCT05203939, A phase 1/2 study to assess the safety and efficacy of OCU400 for retinitis pigmentosa associated with NR2E3 and RHO mutations and leber congenital amaurosis with mutation(s)" in *CEP290Gene* (2023).
35. S. Böhm *et al.*, A gene therapy for inherited blindness using dCas9-VPR–mediated transcriptional activation. *Sci. Adv.* **6**, eaba5614 (2020).
36. R. S. Finkel *et al.*, Nusinersen versus sham control in infantile-onset spinal muscular atrophy. *N. Engl. J. Med.* **377**, 1723–1732 (2017).
37. T. M. Miller *et al.*, Trial of antisense Oligonucleotide Tofersen for SOD1 ALS. *N. Engl. J. Med.* **387**, 1099–1110 (2022).
38. S. A. Ramsbottom *et al.*, Targeted exon skipping of a CEP290 mutation rescues Joubert syndrome phenotypes in vitro and in a murine model. *Proc. Natl. Acad. Sci. U.S.A.* **115**, 12489–12494 (2018).
39. R. J. Platt *et al.*, CRISPR-Cas9 knockin mice for genome editing and cancer modeling. *Cell* **159**, 440–455 (2014).
40. S.-H. Chiou *et al.*, Pancreatic cancer modeling using retrograde viral vector delivery and in vivo CRISPR/Cas9-mediated somatic genome editing. *Genes Dev.* **29**, 1576–1585 (2015).
41. B. Chang *et al.*, A homologous genetic basis of the murine cpfl1 mutant and human achromatopsia linked to mutations in the PDE6C gene. *Proc. Natl. Acad. Sci. U.S.A.* **106**, 19581–19586 (2009).
42. Y. Li, J. Kim, Distinct roles of neuronal and microglial CB2 cannabinoid receptors in the mouse hippocampus. *Neuroscience* **363**, 11–25 (2017).
43. N. E. Sanjana, O. Shalem, F. Zhang, Improved vectors and genome-wide libraries for CRISPR screening. *Nat. Methods* **11**, 783–784 (2014).
44. D. Dalkara *et al.*, AAV mediated GDNF secretion from retinal glia slows down retinal degeneration in a rat model of retinitis pigmentosa. *Mol. Ther.: J. Am. Soc. Gene Ther.* **19**, 1602–1608 (2011).
45. D. F. Wozniak *et al.*, Apoptotic neurodegeneration induced by ethanol in neonatal mice is associated with profound learning/memory deficits in juveniles followed by progressive functional recovery in adults. *Neurobiol. Dis.* **17**, 403–414 (2004).
46. K. Clement *et al.*, CRISPResso2 provides accurate and rapid genome editing sequence analysis. *Nat. Biotechnol.* **37**, 224–226 (2019).
47. A. Dobin *et al.*, STAR: Ultrafast universal RNA-seq aligner. *Bioinform. (Oxford, England)* **29**, 15–21 (2013).
48. S. Anders, P. T. Pyl, W. Huber, HTSeq–a Python framework to work with high-throughput sequencing data. *Bioinform. (Oxford, England)* **31**, 166–169 (2015).
49. M. I. Love, W. Huber, S. Anders, Moderated estimation of fold change and dispersion for RNA-seq data with DESeq2. *Genome Biol.* **15**, 550 (2014).
50. C. M. Chen, C. L. Cepko, Expression of Chx10 and Chx10-1 in the developing chicken retina. *Mech. Dev.* **90**, 293–297 (2000).
51. D. P. Murphy, J. C. Corbo, The effect of acute knockout of Nr2e3 on mouse photoreceptor cells. Gene Expression Omnibus. https://www.ncbi.nlm.nih.gov/geo/query/acc.cgi?acc=GSE256407. Deposited 22 February 2024.
52. D. P. Murphy, C. L. Montana, Y. Liu, J. C. Corbo, Expression data from whole mouse retina comparing acute Nrl knockout and control. Gene Expression Omnibus. https://www.ncbi.nlm.nih.gov/geo/query/acc.cgi?acc=GSE256408. Deposited 22 February 2024.